

Photon Electroproduction from Hydrogen at Backward Angles and Momentum Transfer Squared of $Q^2 = 1.0 \text{ GeV}^2$

G. Laveissière,¹ N. Degrande,² S. Jaminion,¹ C. Jutier,^{1,3} L. Todor,³ R. Di Salvo,¹ L. Van Hoorebeke,² L.C. Alexa,⁴ B.D. Anderson,⁵ K.A. Aniol,⁶ K. Arundell,⁷ G. Audit,⁸ L. Auerbach,⁹ F.T. Baker,¹⁰ M. Baylac,⁸ J. Berthot,¹ P.Y. Bertin,¹ W. Bertozzi,¹¹ L. Bimbot,¹² W.U. Boeglin,¹³ E.J. Brash,⁴ V. Breton,¹ H. Breuer,¹⁴ E. Burtin,⁸ J.R. Calarco,¹⁵ L.S. Cardman,¹⁶ C. Cavata,⁸ C.-C. Chang,¹⁴ J.-P. Chen,¹⁶ E. Chudakov,¹⁶ E. Cisbani,¹⁷ D.S. Dale,¹⁸ C.W. de Jager,¹⁶ R. De Leo,¹⁹ A. Deur,^{1,16} N. d'Hose,⁸ G.E. Dodge,³ J.J. Domingo,¹⁶ L. Elouadrhiri,¹⁶ M.B. Epstein,⁶ L.A. Ewell,¹⁴ J.M. Finn,⁷ K.G. Fissum,¹¹ H. Fonvieille,¹ G. Fournier,⁸ B. Frois,⁸ S. Frullani,¹⁷ C. Furget,²⁰ H. Gao,¹¹ J. Gao,¹¹ F. Garibaldi,¹⁷ A. Gasparian,^{21,18} S. Gilad,¹¹ R. Gilman,^{22,16} A. Glamazdin,²³ C. Glashauser,²² J. Gomez,¹⁶ V. Gorbenko,²³ P. Grenier,¹ P.A.M. Guichon,⁸ J.O. Hansen,¹⁶ R. Holmes,²⁴ M. Holtrop,¹⁵ C. Howell,²⁵ G.M. Huber,⁴ C.E. Hyde-Wright,³ S. Incerti,⁹ M. Iodice,¹⁷ J. Jardillier,⁸ M.K. Jones,⁷ W. Kahl,²⁴ S. Kamalov,²⁶ S. Kato,²⁷ A.T. Katramatou,⁵ J.J. Kelly,¹⁴ S. Kerhoas,⁸ A. Ketikyan,²⁸ M. Khayat,⁵ K. Kino,²⁹ S. Kox,²⁰ L.H. Kramer,¹³ K.S. Kumar,³⁰ G. Kumbartzki,²² M. Kuss,¹⁶ A. Leone,³¹ J.J. LeRose,¹⁶ M. Liang,¹⁶ R.A. Lindgren,³² N. Liyanage,¹¹ G.J. Lolos,⁴ R.W. Lourie,³³ R. Madey,⁵ K. Maeda,²⁹ S. Malov,²² D.M. Manley,⁵ C. Marchand,⁸ D. Marchand,⁸ D.J. Margaziotis,⁶ P. Markowitz,¹³ J. Marroncle,⁸ J. Martino,⁸ K. McCormick,³ J. McIntyre,²² S. Mehrabyan,²⁸ F. Merchez,²⁰ Z.E. Meziani,⁹ R. Michaels,¹⁶ G.W. Miller,³⁰ J.Y. Mougey,²⁰ S.K. Nanda,¹⁶ D. Neyret,⁸ E.A.J.M. Offermann,¹⁶ Z. Papandreou,⁴ C.F. Perdrisat,⁷ R. Perrino,³¹ G.G. Petratos,⁵ S. Platchkov,⁸ R. Pomatsalyuk,²³ D.L. Prout,⁵ V.A. Punjabi,³⁴ T. Pussieux,⁸ G. Quémenér,^{1,7} R.D. Ransome,²² O. Ravel,¹ J.S. Real,²⁰ F. Renard,⁸ Y. Roblin,¹ D. Rowntree,¹¹ G. Rutledge,⁷ P.M. Rutt,²² A. Saha,¹⁶ T. Saito,²⁹ A.J. Sarty,³⁵ A. Serdarevic,^{4,16} T. Smith,¹⁵ G. Smirnov,¹ K. Soldi,³⁶ P. Sorokin,²³ P.A. Souder,²⁴ R. Suleiman,¹¹ J.A. Templon,¹⁰ T. Terasawa,²⁹ L. Tiator,²⁶ R. Tieulent,²⁰ E. Tomasi-Gustafsson,⁸ H. Tsubota,²⁹ H. Ueno,²⁷ P.E. Ulmer,³ G.M. Urciuoli,¹⁷ R. Van De Vyver,² R.L.J. Van der Meer,^{16,4} P. Vernin,⁸ B. Vlahovic,^{16,36} H. Voskanyan,²⁸ E. Voutier,²⁰ J.W. Watson,⁵ L.B. Weinstein,³ K. Wijesooriya,⁷ R. Wilson,³⁷ B.B. Wojtsekhowski,¹⁶ D.G. Zainea,⁴ W-M. Zhang,⁵ J. Zhao,¹¹ and Z.-L. Zhou¹¹

(The Jefferson Lab Hall A Collaboration)

¹Université Blaise Pascal/IN2P3, F-63177 Aubière, France

²University of Gent, B-9000 Gent, Belgium

³Old Dominion University, Norfolk, VA 23529

⁴University of Regina, Regina, SK S4S 0A2, Canada

⁵Kent State University, Kent OH 44242

⁶California State University, Los Angeles, CA 90032

⁷College of William and Mary, Williamsburg, VA 23187

⁸CEA Saclay, F-91191 Gif-sur-Yvette, France

⁹Temple University, Philadelphia, PA 19122

¹⁰University of Georgia, Athens, GA 30602

¹¹Massachusetts Institute of Technology, Cambridge, MA 02139

¹²Institut de Physique Nucléaire, F-91406 Orsay, France

¹³Florida International University, Miami, FL 33199

¹⁴University of Maryland, College Park, MD 20742

¹⁵University of New Hampshire, Durham, NH 03824

¹⁶Thomas Jefferson National Accelerator Facility, Newport News, VA 23606

¹⁷INFN, Sezione Sanità and Istituto Superiore di Sanità, 00161 Rome, Italy

¹⁸University of Kentucky, Lexington, KY 40506

¹⁹INFN, Sezione di Bari and University of Bari, 70126 Bari, Italy

²⁰Laboratoire de Physique Subatomique et de Cosmologie, F-38026 Grenoble, France

²¹Hampton University, Hampton, VA 23668

²²Rutgers, The State University of New Jersey, Piscataway, NJ 08855

²³Kharkov Institute of Physics and Technology, Kharkov 61108, Ukraine

²⁴Syracuse University, Syracuse, NY 13244

²⁵Duke University, Durham, NC 27706

²⁶Institut fuer Kernphysik, University of Mainz, D-55099 Mainz, Germany

²⁷Yamagata University, Yamagata 990, Japan

²⁸Yerevan Physics Institute, Yerevan 375036, Armenia

²⁹Tohoku University, Sendai 980, Japan

³⁰Princeton University, Princeton, NJ 08544

³¹INFN, Sezione di Lecce, 73100 Lecce, Italy

³²University of Virginia, Charlottesville, VA 22901³³State University of New York at Stony Brook, Stony Brook, NY 11794³⁴Norfolk State University, Norfolk, VA 23504³⁵Florida State University, Tallahassee, FL 32306³⁶North Carolina Central University, Durham, NC 27707³⁷Harvard University, Cambridge, MA 02138

We have made the first measurements of the $ep \rightarrow ep\gamma$ exclusive reaction at $Q^2 = 1 \text{ GeV}^2$ in the nucleon resonance region. The cross section is obtained at CM backward angle $\theta_{\gamma\gamma}^*$, in a range of total (γ^*p) CM energy W from the proton mass up to $W = 1.95 \text{ GeV}$. The data show resonant structures in the first and second resonance regions, and is well reproduced at higher W by the Bethe-Heitler+Born cross section, including t-channel π^0 exchange. A comparison is made with existing data in Real Compton Scattering at high W . Our measurement of the ratio of $H(e, e'p)\gamma$ to $H(e, e'p)\pi^0$ cross sections is presented and compared to model predictions.

PACS numbers: 13.60.-r, 13.60.Fz

Understanding nucleon structure in terms of the non-perturbative dynamics of quarks and gluons requires new and diverse experimental data to guide theoretical approaches and to constrain models. Purely electro-weak processes are privileged tools since they can be interpreted directly in terms of the current carried by the quarks. This has motivated an extensive program of elastic, inelastic, and deep inelastic lepton and photon scattering experiments on the nucleon. This Letter presents a study of the nucleon resonance region via the photon electroproduction reaction: $H(e, e'p)\gamma$. For the first time, we separate this process from the more abundant $H(e, e'p)\pi^0$ reaction, and extract the ratio of the two cross sections.

The Constituent Quark Model of N. Isgur and G. Karl [1] reproduces many features of the nucleon spectrum. However, for $W > 1.6 \text{ GeV}$, the model predicts a number of positive parity resonances [2] that have not been seen experimentally. The simultaneous study of both $(N\pi)$ and $(N\gamma)$ final states of the electroproduction process on the nucleon offers a probe with very different sensitivity to the resonance structures. Another motivation for the present study is to explore the exclusive $ep \rightarrow ep\gamma$ reaction at high W , where current quark degrees of freedom may become as important as those of constituent quarks in the understanding of resonances. Quark-hadron duality implies that even at modest Q^2 , inelastic electron scattering in the resonance region can be analyzed in terms of quark degrees of freedom in the t -channel of the forward Compton amplitude instead of nucleon resonances in the s -channel [3].

We define the kinematics of the $ep \rightarrow ep\gamma$ reaction in Fig. 1a. A common set of invariant kinematic variables is defined as $-Q^2 = (k - k')_\mu = q_\mu^2$, $s = W^2 = (q + p)_\mu^2$, $t = (p - p')_\mu^2$, and $u = (p - q')_\mu^2$; $\theta_{\gamma\gamma}^*$ and $\phi_{\gamma\gamma}$ are the polar and azimuthal angles in the $\gamma^*p \rightarrow \gamma p$ subprocess center of mass (CM) frame. The $ep \rightarrow ep\gamma$ reaction was measured below pion threshold at MAMI ($Q^2 = 0.33 \text{ GeV}^2$) [4] and at the Thomas Jefferson National Accelerator Facility (JLab) ($Q^2 = 0.92$ and 1.76 GeV^2) [5]. We present in this letter the first mea-

surements of the nucleon excitation up to $W = 1.95 \text{ GeV}$ at $Q^2 = 1 \text{ GeV}^2$ through the $ep \rightarrow ep\gamma$ process in CM backward kinematics (\vec{q}' opposite to \vec{q}).

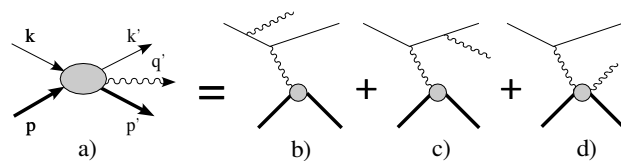


FIG. 1: Kinematics for photon electro-production on the proton (a) and lowest order amplitudes for Bethe-Heitler (b,c) and VCS (d) processes. The incident and scattered electron 4-momenta are k and k' , respectively. The initial and recoil proton 4-momenta are p and p' , and the produced real photon 4-momentum is q' .

In the one photon exchange approximation, the $ep \rightarrow ep\gamma$ amplitude (Fig. 1a) includes the coherent superposition of both the Bethe-Heitler (BH) amplitude (Fig. 1b and 1c) [6], and the VCS amplitude $\gamma^*p \rightarrow \gamma p$ (Fig. 1d). Notice that in the BH amplitude, the mass of the virtual photon (elastically absorbed by the proton) is t . In the VCS amplitude, the mass of the virtual photon (inelastically absorbed) is $-Q^2$. The BH amplitude dominates over the VCS when the photon is emitted in either the direction of the incident or scattered electron. It is important to note that the BH amplitude breaks the symmetry of the electroproduction amplitude around the virtual photon direction. Thus, it is not possible to expand the $ep \rightarrow ep\gamma$ cross section in terms of longitudinal and transverse (L,T) photoproduction cross sections, except when the BH amplitude is really negligible. Although the VCS amplitude is the dominant contribution to the $ep \rightarrow ep\gamma$ process in our kinematics, we did not perform an L-T separation: at low W the interference between BH and the VCS Born term is not negligible; and at higher W the experimental statistics is low.

The experiment was performed at JLab in Hall A. The continuous electron beam of energy $k = 4.032 \text{ GeV}$ with an intensity of 60-120 μA was sent onto a liquid hydro-

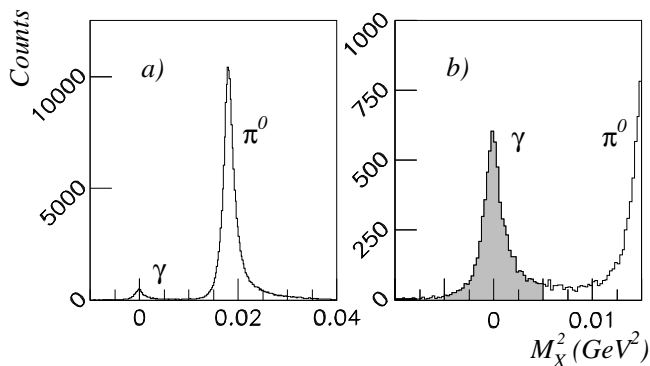


FIG. 2: Squared missing mass $M_X^2 = (k + p - k' - p')^2$ for an experimental setting at $W = 1.2$ GeV (a) and zoom around the γ peak (b). The $[-0.005, 0.005 \text{ GeV}^2]$ window is used to separate the γ events from the π^0 events.

gen target. The scattered electron and recoil proton were detected in coincidence in two high resolution spectrometers equipped with drift chambers and plastic scintillator hodoscopes. The emitted photon was reconstructed using a missing particle technique. A spectrum of the squared missing mass $M_X^2 = (k + p - k' - p')^2$ is displayed in Fig 2. A detailed description of the apparatus and detector acceptance is given in [7], [8] and [9].

We extract the 5-fold differential cross section $d^5\sigma = d^5\sigma/dk'_{lab}d[\Omega_e]_{lab}d[\Omega_p]_{CM}$ using the method described in [8]; dk'_{lab} and $d[\Omega_e]_{lab}$ are the scattered electron differential momentum and solid angle in the lab frame, and $d[\Omega_p]_{CM}$ is the proton CM differential solid angle. The calculation of the solid angle and radiative corrections is based on a simulation [10] of the coherent sum of the BH and VCS amplitudes. The VCS amplitude is approximated by the Born term only, which corresponds to the $\gamma^*p \rightarrow \gamma p$ process in which the intermediate state is an on-shell proton in the s - or u -channels.

Several experimental corrections are applied for each sequence of the data. They concern the acceptance, the trigger efficiency, the acquisition and electronic dead times, the tracking efficiency, the target boiling, the target impurity, the integrated charge and the proton absorption [8]. In this analysis, we have to consider some additional specific corrections. The π^0 events remaining in the M_X^2 window $[-0.005, 0.005 \text{ GeV}^2]$ used to define the γ events have to be subtracted. Their amount is estimated from the simulation, using as a weight of the $ep \rightarrow ep\pi^0$ events the MAID2000 calculation [11]. The correction remains small (-0.1 to -1.7%). The systematic and statistical errors on the cross sections depend on W and range from 10 to about 50 %. The method used to estimate the systematic error is described in [5].

In Fig. 3 we present the 5-fold differential cross sections $d^5\sigma$ for the six bins in $\phi_{\gamma\gamma}$ (30° wide) as a function of W , at $Q^2 = 1 \text{ GeV}^2$ and $\cos\theta_{\gamma\gamma}^* = -0.975$. By symmetry, the statistics from $\phi_{\gamma\gamma} = 0$ to -180° are also included.

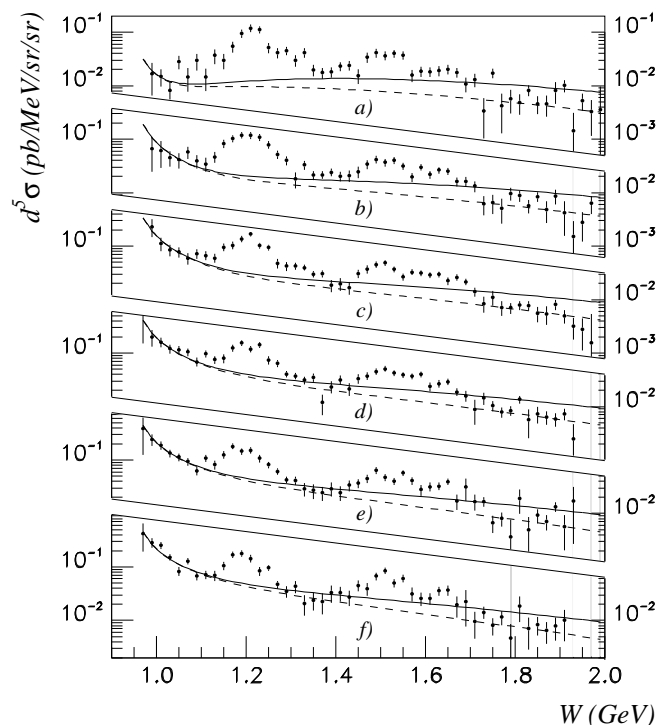


FIG. 3: Excitation curves for $ep \rightarrow ep\gamma$ at $Q^2 = 1 \text{ GeV}^2$, $\cos\theta_{\gamma\gamma}^* = -0.975$ and $\phi_{\gamma\gamma} = 15^\circ$ (a), 45° (b), 75° (c), 105° (d), 135° (e) and 165° (f). The full line is the BH+Born cross section, and the dashed line is the BH+Born+ π^0 cross section [12] (see text).

Additional points as well as the exact binning are available in [13]. The data show strong resonance phenomena in the first and second resonance regions.

Real Compton scattering (RCS) has been intensively investigated in the $\Delta(1232)$ -resonance [14] and in the high energy diffractive region [15]. RCS was also studied above the $\Delta(1232)$ at Bonn [16], Saskatoon [17], and Tokyo [18, 19]. The Cornell experiment [20] measured the RCS process at photon energies E_γ from 2–6 GeV and angles from 45° to 128° in the CM frame. A recent Jefferson Lab experiment [21] measured the RCS process at E_γ from 3–6 GeV. In Fig. 4, we compare our backward angle $ep \rightarrow ep\gamma$ cross section divided by the photon flux factor (Hand convention [8]) with existing large angle RCS data. For comparison purposes, all our cross sections are averaged over the azimuthal angle $\phi_{\gamma\gamma}$.

Our data in Figs. 3 and 4 at high W surprisingly approach the BH+Born cross section if we include the t -channel π^0 exchange diagram [12] (denoted by BH+Born+ π^0). This can be interpreted by the resonance model of Capstick and Keister [22]: for RCS, at backward angles all positive parity intermediate states contribute constructively and all negative parity states contribute destructively. If there are no diffractive minima (as a function of Q^2) in the resonance form factors, this effect will remain in the VCS amplitude. Moreover,

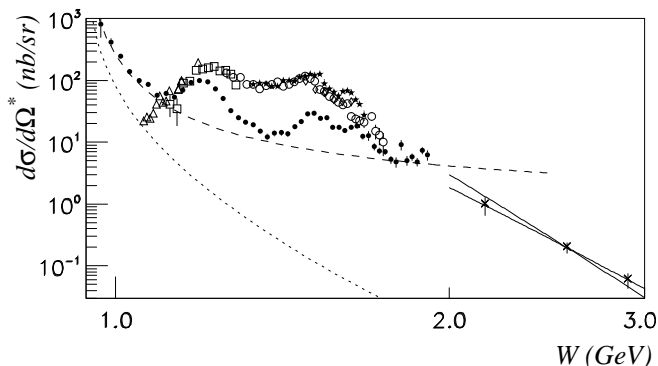


FIG. 4: Comparison of VCS data (\bullet) (this expt) at $\theta_{\gamma\gamma}^* = 167.2^\circ$ and RCS data at $\theta_{\gamma\gamma}^* = 159 - 162^\circ$ (\star) [18], $\theta_{\gamma\gamma}^* = 128 - 132^\circ$ (\diamond) [16], $\theta_{\gamma\gamma}^* = 141^\circ$ (\triangle) [17], $\theta_{\gamma\gamma}^* = 130 - 133^\circ$ (\circ) [19], $\theta_{\gamma\gamma}^* = 131^\circ$ (\square) [14] and $\theta_{\gamma\gamma}^* = 105 - 128^\circ$ (\times) [20]. The solid curves are s^{-6} and s^{-7} power laws, normalized to the $W = 2.55$ GeV Cornell point. The dashed curve is the BH+Born+ π^0 cross section [12] and the dotted curve the BH alone.

at high W and wide angles ($-t$ and $-u$ large), the RCS cross section is governed by a scaling law [23]: the counting rules predict that $d\sigma/dt$ scales as s^{-6} at fixed CM scattering angle (see Fig. 4). The Cornell data [20] is roughly independent of angle for $\theta_{\gamma\gamma}^* \geq 90^\circ$ and scales as $s^{-7.1 \pm 0.4}$ at $\theta_{\gamma\gamma}^* = 90^\circ$. At large s , the VCS Born amplitude (Fig. 4) is determined by the Q^2 -dependent proton form factors and the u -channel proton exchange, whereas the scaling law is dominated by the t -dependent Compton form factor [24, 25]. In our kinematics since $-t \gg Q^2$, $-u$, the perturbative Compton cross section is smaller than the Born cross section, equivalently the negative parity s -channel resonances should overcompensate the positive parity resonances. New backward angle VCS data at large W would provide a powerful test of the Born-term versus s^{-6} scaling. We consider the agreement between our data and RCS in the region of $W \sim 1.8$ GeV (see Fig. 4) as an evidence of the suppression of the Q^2 dependence of the VCS cross sections. This is consistent with the quark-hadron duality picture, according to which photons from both RCS and VCS processes couple at high W to current quarks rather than to individual nucleon resonances.

From these results and the results presented in [8], we have computed the ratio between the $ep \rightarrow ep\gamma$ and $ep \rightarrow ep\pi^0$ cross sections at $\cos\theta_{\gamma\gamma}^* = -0.975$ and $Q^2 = 1$ GeV 2 for the entire resonance region. In Fig. 5 we show the value of the ratio averaged over the six bins in $\phi_{\gamma\gamma}$. In the range extending from the reaction threshold up to $W = 1.6$ GeV, the result is consistently a factor 10 larger than the ratio of the branching fractions of any corresponding resonance into (γN) and (πN) . In the region of the P_{33} Δ -resonance, the experimental ratio is five times larger than the [BH+Born+ π^0]/MAID2000 [11] calculation. Thus one has to be careful when correcting

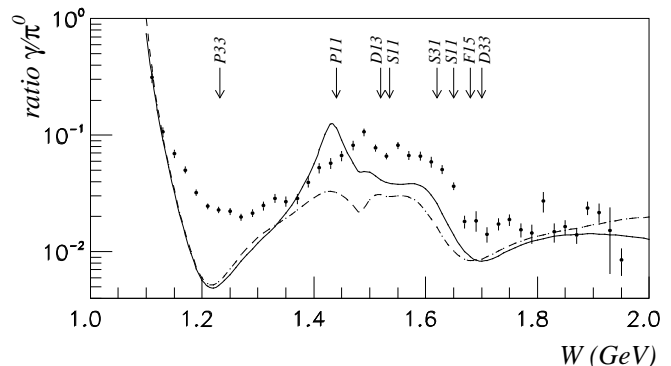


FIG. 5: Ratio of $ep \rightarrow ep\gamma$ over $ep \rightarrow ep\pi^0$ cross sections at $Q^2 = 1$ GeV 2 and $\theta_{\gamma\gamma}^* = 167.2^\circ$. The full and dashed curves are the ratios between the BH+Born+ π^0 cross section and the MAID2000 model [11] and the MAID2003 *local fit* of [8] respectively.

$H(e, e'p)\pi^0$ experiments if the resolution does not allow a clear separation of the $H(e, e'p)\gamma$ channel. Our results illustrate that both the VCS and π^0 production amplitudes result from a distinct coherent superposition of all intermediate states.

We wish to acknowledge the staff of the accelerator who delivered the beam, as well as the Hall A technical staff. This work was supported by DOE contract DE-AC05-84ER40150 under which the Southeastern Universities Research Association (SURA) operates the Thomas Jefferson National Accelerator Facility. We acknowledge additional grants from the US DOE and NSF, the French Centre National de la Recherche Scientifique and Commissariat à l'Énergie Atomique, the Conseil Régional d'Auvergne, the FWO-Flanders (Belgium) and the BOF-Gent University.

-
- [1] N. Isgur and G. Karl, Phys. Rev. **D19**, 2653 (1979).
 - [2] R. Koniuk and N. Isgur, Phys. Rev. Lett. **44**, 845 (1980).
 - [3] I. Niculescu et al., Phys. Rev. Lett. **85**, 1186 (2000).
 - [4] J. Roche et al., Phys. Rev. Lett. **85**, 708 (2000).
 - [5] S. Jaminion et al. (JLab Hall A) (2004), to be published in Phys. Rev. Lett., hep-ph/0404243.
 - [6] H. Bethe and W. Heitler, Proc. Roy. Soc. Lond. **A146**, 83 (1934).
 - [7] J. Alcorn et al., Nucl. Instrum. Meth. **A522**, 294 (2004).
 - [8] G. Laveissiere et al. (JLab Hall A), Phys. Rev. **C69**, 045203 (2004), nucl-ex/0308009.
 - [9] G. Laveissiere, Ph.D. thesis, Université Blaise Pascal, Clermont-Fd, France (2001), DU 1309.
 - [10] L. Van Hoorebeke et al., to be submitted to NIM A.
 - [11] D. Drechsel, O. Hanstein, S. S. Kamalov, and L. Tiator, Nucl. Phys. **A645**, 145 (1999), nucl-th/9807001, URL <http://www.kph.uni-mainz.de/MAID/>.
 - [12] M. Vanderhaeghen, Phys. Lett. **B368**, 13 (1996).
 - [13] See EPAPS Document No. for cross section tables. A direct link to this document may be found in

the online article's HTML reference section. The document may also be reached via the EPAPS homepage (<http://www.aip.org/pubservs/epaps.html>) or from <ftp.aip.org> in the directory `/epaps/`. See the EPAPS homepage for more information.

- [14] F. Wissmann et al., Nucl. Phys. **A660**, 232 (1999).
- [15] T. H. Bauer, R. D. Spital, D. R. Yennie, and F. M. Pipkin, Rev. Mod. Phys. **50**, 261 (1978).
- [16] M. Jung et al., Zeit. Phys. **C10**, 197 (1981).
- [17] E. L. Hallin et al., Phys. Rev. **C48**, 1497 (1993).
- [18] Y. Wada et al., Nucl. Phys. **B247**, 313 (1984).
- [19] T. Ishii et al., Nucl. Phys. **B254**, 458 (1985).
- [20] M. A. Shupe et al., Phys. Rev. **D19**, 1921 (1979).
- [21] C. Hyde-Wright, A. Nathan, B. Wojtsekhowski, et al. (1999), experiment E99-114 (Hall A), URL http://www.jlab.org/exp_prog/generated/apphalla.html.
- [22] S. Capstick and B. D. Keister, Phys. Rev. **D47**, 860 (1993), and Phys. Rev. **D46**, 84 (1992).
- [23] S. J. Brodsky and G. R. Farrar, Phys. Rev. **D11**, 1309 (1975).
- [24] A. V. Radyushkin, Phys. Rev. **D58**, 114008 (1998).
- [25] H. W. Huang, P. Kroll, and T. Morii, Eur. Phys. J. **C23**, 301 (2002), hep-ph/0110208.